

## Article

# Features of Degassing from Overburden Rock Massifs: A Case Study Using Radon

Timofey Leshukov <sup>1,\*</sup>, Aleksey Larionov <sup>2</sup>, Ekaterina Nastavko <sup>1</sup>, Philipp Kaizer <sup>1</sup> and Konstantin Legoshchin <sup>1</sup>

<sup>1</sup> Department of Geology and Geography, Institute of Biology, Ecology and Natural Resources, Kemerovo State University, 6 Krasnaya Street, 650000 Kemerovo, Russia; evnastavko@yandex.ru (E.N.); filipp.kaizer@yandex.ru (P.K.); geology@kemsu.ru (K.L.)

<sup>2</sup> Department of Genetics and Fundamental Medicine, Institute of Biology, Ecology and Natural Resources, Kemerovo State University, 6 Krasnaya Street, 650000 Kemerovo, Russia; larionov@kemsu.ru

\* Correspondence: tvleshukov@kemsu.ru

**Abstract:** Overburden rock massifs resulting from open-pit coal mining are very common objects in the world's mining regions. These locations pose a significant challenge as the global mining industry expands. These dumps are capable of self-burning for quite a long time. The displacement and sliding of these massifs can cause catastrophic consequences. In addition, these objects emit a significant amount of greenhouse gases into the atmosphere. Therefore, it is necessary to manage such objects and implement appropriate measures to limit their impact on the environment. In this work, we studied soil radon volume activity (VAR) and radon flux density (RFD) on the surface of the overburden rock massif of coal-bearing mining rocks and also made visual fixation of disturbances in the body of the massif, which appeared in the process of its movement. We found anomalies of VAR and RFD on the surface of the overburden extending from north to south. These anomalies were extended along the strike of the faults found in the body of the massif. Additionally, the radon anomalies coincided with the anomalies of methane gas emission previously measured for this object. Thus, we determined that the exit of gases from the body of the massif is carried out through fault (weakened) zones in the body of the massif. According to the results of the study, we propose to carry out radon monitoring in order to detect the spontaneous ignition process of the massif or the increase of its mobility. This will also allow us to take appropriate measures to stabilize the massif or to extinguish the dump before or simultaneously with the biological stage of reclamation.



**Citation:** Leshukov, T.; Larionov, A.; Nastavko, E.; Kaizer, P.; Legoshchin, K. Features of Degassing from Overburden Rock Massifs: A Case Study Using Radon. *Earth* **2024**, *5*, 1–19. <https://doi.org/10.3390/earth5010001>

Academic Editor: Carlito Tabelin

Received: 22 November 2023

Revised: 11 December 2023

Accepted: 21 December 2023

Published: 25 December 2023



**Copyright:** © 2023 by the authors. Licensee MDPI, Basel, Switzerland. This article is an open access article distributed under the terms and conditions of the Creative Commons Attribution (CC BY) license (<https://creativecommons.org/licenses/by/4.0/>).

## 1. Introduction

The preparation and operation of an open-pit coal mine produce a certain amount of rock that is disposed of in a designated area within the license area or elsewhere, depending on the mining project [1]. Most of this rock is classified as overburden. The lithological composition of overburden rocks is similar to that of the rocks of the mined overburden and the overlying younger loose sediments. They differ only in the lower (unconditioned) content of carbonaceous material in the rock layers and are, therefore, not included in the mineral resource. There are various types of overburden placement [2–4]. Two patterns were considered in the present research: a large bulk massif and the distribution of overburden rocks in a shallow-gully network of valleys. The rocks display a wide range of fractional compositions from block to clayey debris [5,6]. Generally, the massif has a somewhat organized composition, characterized by a certain change in the size of the debris from the lower part of the massif to the upper part.

Overburden is a global problem [7–9]. The amount of overburden is increasing. Various researchers are attempting to solve this problem using these breeds in the economy [10–12].

Overburden rocks create many problems for the areas where they are located. One of the problems is the large amount of dust that is formed from overburden rocks during the process of weathering and dispersal by air currents. Dust of various sizes is transported over long distances, polluting environmental components and causing adverse effects on the population [13–15]. Another problem with overburden is its impact on water bodies. These objects change their natural hydrochemical composition and become enriched in toxic substances due to their removal from the body of the massif by precipitation [16–19].

According to previous studies, carbon dioxide, carbon monoxide, methane, radon, and other gases are emitted from the waste massifs of overburden rocks [20,21]. The intensity of gas emission may depend on the fractional composition of rocks that make up the massif, processes occurring in the massif itself (e.g., intense oxidation of carbonaceous rocks), mobility of the massif, and other factors, including meteorological [22]. The volume of gases coming from the overburden massif is generally associated with the processes of underground rock burning, oxidation reaction, and release of radon gas from coal and other rocks [23–26]. The porous structure of the entire waste rock massif, particularly in its early stages, enables excellent aeration and the unhindered flow of gases within it. The migration of some of these gases to the surface can be stimulated by the migration of neighboring gases moving through the massif. For example, radon is released by the migration of methane and hydrogen to the surface [27–29]. Thus, the spatial features of gases coming to the surface and their dynamics can provide important information regarding the oxidative processes occurring inside the massif or suggest dynamic processes in the dump mass. In addition, carbon dioxide, carbon monoxide, and methane are three prominent greenhouse gases. As per sustainable development principles, their emissions must be reduced [30–34]. Additionally, radioactive gases (radon, thoron), which can be harmful to humans, can cause a certain danger [35]. These gases are known to increase carcinogenic risks with prolonged exposure [35].

In order to minimize the impact of the dump on the environment, these objects are subject to reclamation. Waste remediation is carried out in two stages: geological and biological. The first stage involves preparing the lithological base for subsequent biological reclamation. At the biological stage, the soil layer is formed, plants are planted, and the site is restored to an approximation of its natural appearance. The geological stage of reclamation is necessary to prepare the dump mass for the biological stage. Thus, for favorable reclamation, it is necessary that the dump rock mass be stable, both in terms of its mobility and in terms of the processes occurring in it (mainly spontaneous combustion). It is recognized that after the formation of the waste rock massif, it continues its movement for some time due to compaction and sliding of part of the material along the slope and sliding mirrors, then the array can stop [36]. These dynamic processes will presumably be accompanied by changes in the directions of gas migration within the body of the massif. In other words, in one part of the massif body, we will observe an increase in the volume of gases (radon, methane), and in another part, they will decrease. This corresponds to a zone of tension in the first case and to compression in the second. Over time, the waste rock massif can naturally decrease its emissions to the atmosphere as it becomes compacted and covered by loose rock and vegetation. However, this can occur only if the massif's fluidity decreases or movement stops completely.

Thus, radon and methane serve as important indicator gases of the stress-strain state of geological objects, including waste dumps, and can also provide important information regarding the combustion processes inside them. As is known, spontaneous combustion of a dump mass has an adverse effect on the processes of reclamation or self-overgrowth of the dump mass. From this, it follows that if combustion processes in the rock mass are not investigated prior to the biological stages, they can impede the reclamation of the land [37]. Additionally, it should be noted that spontaneous combustion may even occur following the conclusion of reclamation efforts [38–40].

Thus, the presented research is important for open-pit coal mining regions. Kuzbass is a territory where open-pit coal mining technology is a priority, but this is also typical for

other mining countries in the world. The annual increase in coal production is 5–7% [6]. As of 2015, the volume of overburden is 400 Mm<sup>3</sup> from coal mining. The number of dumps in Kuzbass amounts to hundreds of objects [2]. The volume of gas emissions in the process of coal mining is colossal; overburden rocks provide a fairly large share, especially when the process of spontaneous combustion of such objects begins. When the combustion processes of the dump mass are activated, the emission of gases to the surface accelerates and their composition changes.

A decrease in the rate of reclamation of objects with insufficient knowledge of the combustion processes inside the dump mass and its dynamics will lead to an increase in the dust load of such objects, as well as an increase in gas emissions into the atmosphere.

Thus, the objects proposed for study require monitoring of organic combustion processes and dynamic processes. Our research examines the emission of gases from overburden rock massifs. <sup>222</sup>Rn was identified as an indicator gas. The study contributes to comprehending gas migration processes from overburden rock massifs, determines massif stability, and assesses the impact of a dense clay layer on reducing gas release to the surface. Additionally, the acquired findings will enable the elimination of the impact of waste rock massifs burning of the dump on the cultivated botanical communities prior to the initiation of the biological phase of restoration.

## 2. Materials and Methods

Three waste rock massifs were selected as the objects of the study, which differed in the presence of the biological stage of reclamation and the method of overburden disposal. The primary site for the experiment was overburden rock massif (further, «Case») situated near the Talda village, where the area is currently being prepared for the biological stage of reclamation. Additionally, two locations with placed overburden in the vicinity of the cities of Leninsk-Kuznetsky (further, «Control 1») and Berezovsky (further, «Control 2») were selected as comparison territories. The specifics of these sites and research territory are shown in Figure 1.

The waste rock in Control 1 was located along the valleys of the ravine-gullies network. The slopes of the valleys were gentle and composed of loam and clay. The maximum overburden thickness reaches up to 15–20 m, but in some cases, it remains undetermined, primarily in watersheds. The waste rock massifs are characterized by a disorderly rock composition. No significant layer of compacted clay was detected. The site is covered by soil, shrubs, trees, and herbs with a dense turf layer.

Case territory is located in the depression of the river relief exceeding the level of natural heights for this area. The surface is largely free of soil and vegetation. The upper horizon consists of heavy loams and extremely dense clays with interspersed fragments of gravel, broken stone, and boulders. At one point, there is a layer of soil with planted herbaceous vegetation.

Case and Control 2 territory are similar in the way of overburden deposition. Both areas are upland areas with a defined stepped relief. Last partially covered by various species of trees, shrubs, and herbaceous vegetation. No distinct clay layer was found here.

Below is more detailed information on Case territory [41,42]. Tectonically, the study area belongs to the Alatau zone of the Kuznetsk coal basin. Beneath the Cenozoic deposits are Paleozoic rock complexes dating back to the Permian period. In general, the formations are represented by cyclites of different scales and consist of rhythmically interbedded sandstones, siltstones of different grain sizes, and coals. Mudstones and limestones have a subordinate and limited distribution in the sequence. Cenozoic deposits are represented mainly by loams and clays. The thickness of sediments increases towards the watersheds of rivers and ravines.

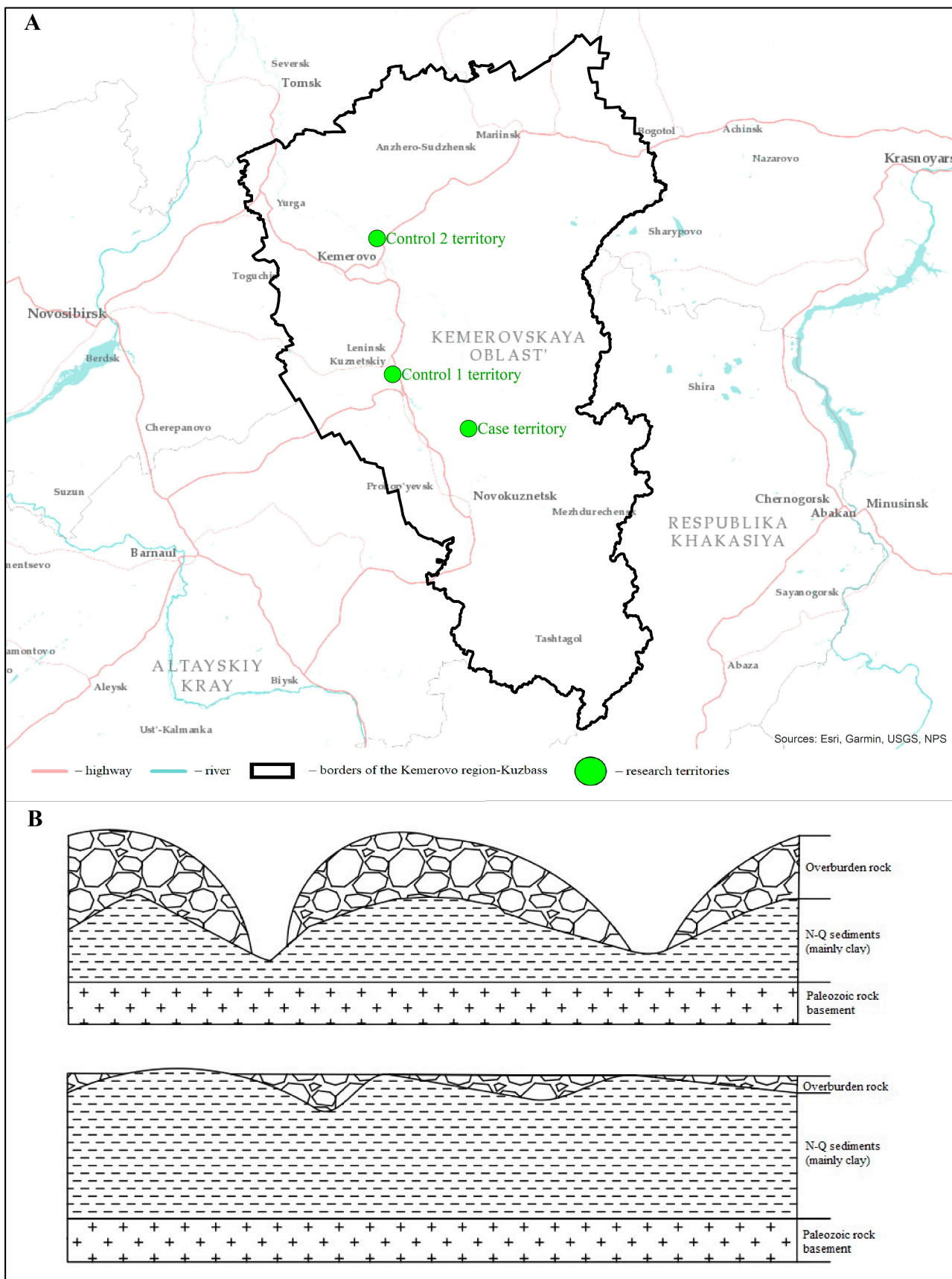


**Figure 1.** Research territory (A) and scheme of overburden placement options being explored (above is Case and Control 2, below is Control 1) (B).

Previously, a value for radioactive elements content in the upper rock horizon was obtained for the Case territory. The range of  $^{232}\text{Th}$  content was 30.78 to 38.4 Bq/kg, with a mean value of  $36.02 \pm 1.38$  Bq/kg. The background value recorded was 32.2 Bq/kg.  $^{226}\text{Ra}$  content ranged from 19 to 31.6 Bq/kg, with a mean value of  $24.1 \pm 2.08$  Bq/kg. The background value was below 20 Bq/kg. Therefore, these territories are not contaminated with radioactive elements according to contemporary normative (100 Bq/kg for  $^{226}\text{Ra}$ ). Moreover, the sufficiently homogeneous distribution of radioactive elements in the upper horizon of the rock excludes the influence of this factor on soil radon and radon flux density.

The overburden rock massifs area was also surveyed for temperature anomalies to exclude the presence of underground fires. Infrared imagery was taken using a Matrice 300 RTK (SZ DJI Technology Co., Ltd., Shenzhen, China). Weather conditions: wind 3 m/s and temperature 5 °C. The flight altitude was 100 m relative to the terrain. The flight was performed with terrain enveloping. Figure 2 shows a section of the map of the study area with isolines of absolute surface temperature.

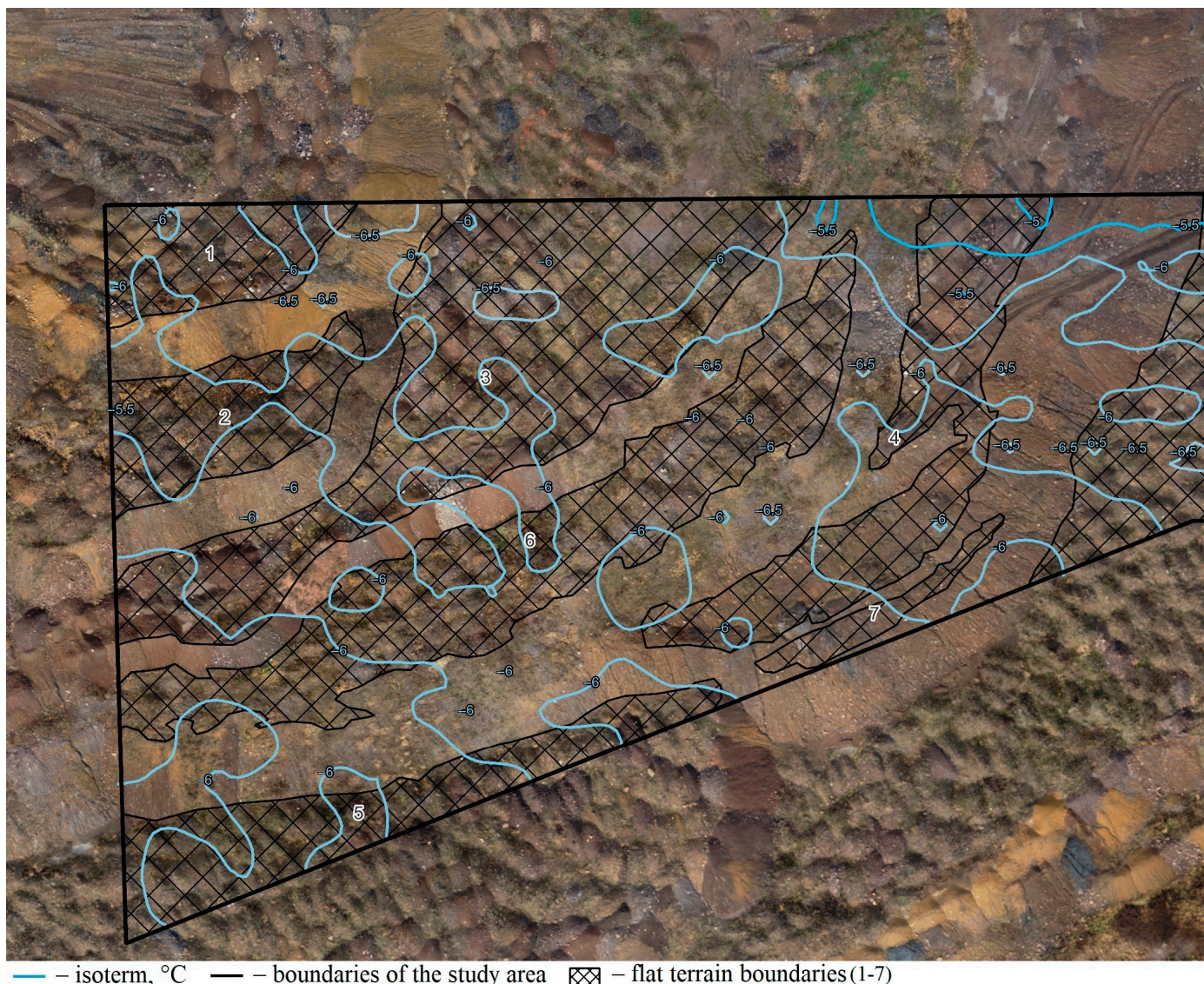


**Figure 2.** Absolute temperature isotherms of the massif surface (scale 1:2000).

Max and min temperatures of  $-5.5^{\circ}\text{C}$  and  $-6.5^{\circ}\text{C}$ , respectively, were observed, with a low amplitude and gradient. The absence of significant temperature gradients suggests the absence of current carbon-containing product combustion processes within the massif [43,44]. Since heating spots are usually located at depths of 1.5–2.5 m or up to 5 m, the data indicate the absence of combustion processes in the dump [21].

The study area was also examined for methane leaks from the massif (Figure 3). A remote laser methane detector, Laser Methane mini, from a Matrice 210 RTK drone (SZ DJI Technology Co., Ltd., Shenzhen, China), was used for the study. The device's measurement ranged from 1 to 50,000 ppm, with a possible error of up to 10%. The aerial survey was conducted under specific weather conditions: wind speed of 3 m/s and an ambient temperature of  $-5^{\circ}\text{C}$ .

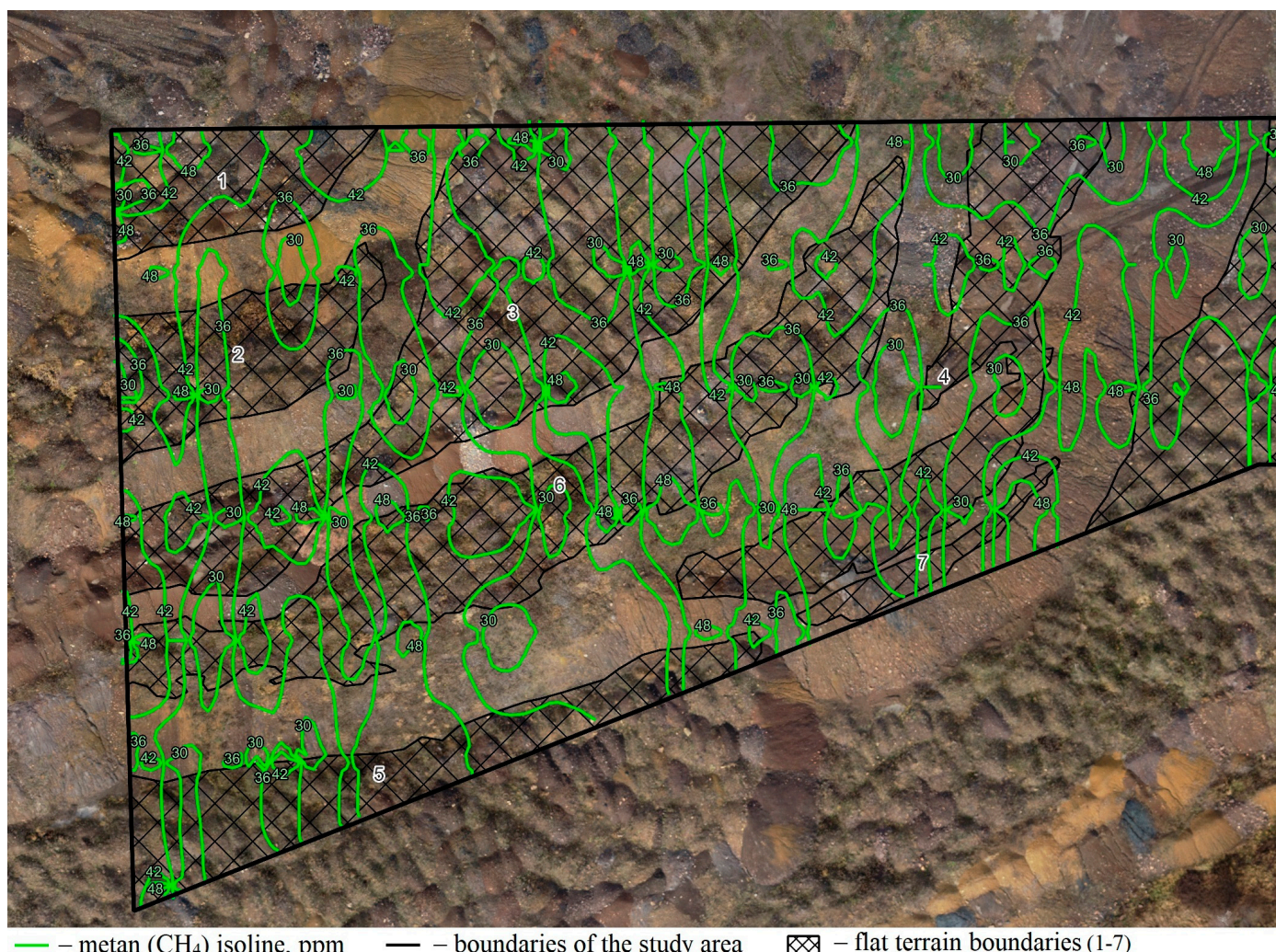


**Figure 3.** Methane leakage isolines from the Case territory (scale 1:2000).

The values ranged between 30 and 48 ppm. According to the obtained map, it is possible to assume the presence of methane outlets to the surface through permeable zones. Most likely, they are formed by fracture zones due to the displacement of the massif body in the process of its first movement. Hence, the primary factor that affects surface radon concentration is the gas permeability of the massif and underlying rocks.

## 2.1. VAR and RFD Measurement

Radon flux density (RFD, 135 sample sites) and soil radon volume activity (VAR, 9 sample sites) were measured at the Control 1 territory. The Case territory was also measured (50 and 10 sample sites, respectively). RFD was measured at the Control 2 territory (45 sample sites with no VAR).

Below is a brief description of the method for assessing VAR. The measurement of VAR in soil air is based on taking a sample of soil air from a hole into a sampler. Determination of VAR in the sampler was determined by mixing the sample between the volumes of the sampler and the measuring chamber and subsequent measurement in the measuring chamber of the measuring unit of the device. Measurement of the volumetric activity of  $^{222}\text{Rn}$  is based on the electrostatic deposition of charged  $^{218}\text{Po}$  (RaA) ions from a selected air sample onto the surface of a semiconductor detector (SD). The volumetric activity of  $^{222}\text{Rn}$  was determined by the number of registered alpha particles during the decay of RaA atoms deposited on the SD. The measuring chamber of the VAR measurement unit is made of plastic and is a hollow cylinder with a high-voltage electrode located inside and hermetically sealed flanges on both sides. Air sampling into the measuring chamber is carried out using a micro-blower in the device. The air sample enters the measuring chamber through a protective aerosol filter, passes through the climate chamber, and enters the micro-blower. A protective aerosol filter is used to purify controlled air from the dispersed phase of aerosols and, in particular, from the SD of radon and thoron in the air. The range of VAR measurements in soil air samples is from  $10^3$  to  $10^6 \text{ Bq/m}^3$ . When taking air samples, the following conditions are observed: the ambient air temperature in the range of  $10^\circ\text{C}$  to  $50^\circ\text{C}$ ; relative humidity up to 100% at an air temperature of  $25^\circ\text{C}$ . The measurement in the chamber is carried out within 30 min. The calculation of radon content in soil was made using the formula:

$$Q_{SA} = Q * \left(1 + \frac{V_2}{V_1} \times \exp(\lambda_{Rn} \times t)\right), \quad (1)$$

where  $V_2$  is the volume of the measuring chamber of the device, l,  $V_2 = 0/94 \text{ l}$ ;

$V_1$  is the sample volume in sample chamber, l,  $V_1 = 0.046 \text{ l}$ ;

$t$  is the time elapsed from the end of air sampling ( $t_1$ ) to the start of measurements ( $t_2$ ), min;  $t = t_2 - t_1$ ;

$Q$  is the measured VAR by measurement unit,  $\text{Bq/m}^3$ .

The limit of permissible relative error when measuring VAR in soil air is no more than 30%.

In all cases, soil radon was collected at a depth of  $40 \pm 2 \text{ cm}$  from 0.08 m diameter wells. Before soil radon sampling, the wells were isolated from ambient air for 24 h. Soil radon was sampled using an AB-07 air sampler (NTM-Zaschita, Moscow, Russia). Soil air was pumped between the borehole, air sampler, and sample tube (50 mL) through a closed system for 5 min at a rate of 1 L/min. Then, the accumulation chamber was connected to an Alfarad+ radon monitor (NTM-Zaschita, Moscow, Russia), and the radon content in the soil air was measured. The method used allows us to understand how much radon is contained in the soil air. With a regular measurement grid, it is possible to make a spatial assessment of soil radon content and identify areas with high and low values. These areas may be interpreted differently in future studies.

RFD was estimated by the method of sorption on charcoal. For this purpose, the radon monitoring complex "Camera-01" (NTC-NITON, Moscow, Russia) was used. Let us provide a brief description of the method for estimating RFD. The RFD measurement method is based on passive sampling for 1–10 h in an NK-32 storage chamber installed on the ground surface. Inside the NK-32 chamber, there is a working (sorbing) layer of activated carbon, which is poured from the SK-13 before installing the NK-32 chamber on the soil. A protective SK-13 is installed on top of the NK-32, which is necessary to prevent

the entry of radon into the chamber from the ground layer of the atmosphere. RFD is calculated using the formula:

$$\sigma_{Rn} = \frac{\lambda \times A}{f \times S \times \{1 - \exp(-\lambda \times t_{exp})\}}, \quad (2)$$

where A is the radon activity in the coal of the working layer NK-32 at the end of passive sampling, Bq;

$\lambda$  is the radon decay constant, 1/s;

$t_{exp}$  is the duration of coal sampling in chamber NK-32, s;

S is the working surface area NK-32, m<sup>2</sup>;

f is the correction factor taking into account the influence of NK-32 on the test object, rel. units.

The error of this research method does not exceed 30%. The volume of activated carbon in measurements of radon activity in coal is  $12.8 \pm 0.6$  cm<sup>3</sup>. The RFD measurement limit for this equipment ranges from 3 to 100,000 mBq·m<sup>-2</sup>·s<sup>-1</sup>. Air temperature during passive sampling with an NK-32 storage chamber when measuring the average RFD from the Earth's surface ranges from –5 to 40 °C. Relative humidity should be 95% maximum at an air temperature of 30 °C.

Measurement of radon activity in coal using the Camera-01 device is assessed by gamma and beta radiation from short-lived daughter products of radon decay—<sup>214</sup>Pb and <sup>214</sup>Bi (DPR), which are in a state of radioactive equilibrium with radon. In this case, to perform the measurement, the exposed coal is poured from SK-13 into the detection unit BDB-13. This block registers the decay of DPR in activated carbon and compares it with the background for activated carbon before exposure to radon. Sorption of radon released from the soil on coal is carried out in the NK-32 trap for 2–8 h (optimally 5 h). Radon activity analysis is carried out after 4 h to establish the equilibrium of radon with DPR. Measurements on the device are carried out within 30 min.

For this purpose, the charcoal chambers were tightly installed in the previously loosened soil. After exposure, the charcoal was poured into a sorption column (SK-13), tightly closed, and kept for 4 h before measurement. The method allows one to estimate the radon yield of their soil, which provides information for assessing the permeability of soil to radon.

Repeated measurements at the same measuring points were made in 15% of cases, and the results did not exceed the manufacturer's error of 30%, and in most cases, the error was smaller.

## 2.2. Statistical Analysis and Spatial Methods

Statistical analyses were performed with the Statistica 14.0 package (StatSoft, Tulsa, OK, USA). Distributions were tested using Kolmogorov–Smirnov, Liliefors, and Shapiro–Wilk tests. The Mann–Whitney U-test was used to examine the differences in both soil radon VAR and RFD between areas. Statistical significance was accepted at the level of  $p \leq 0.05$ . Spatial research methods were used to construct isolines of soil radon content and radon flux density for the Case territory. The Spline tool was used for interpolation. For RFD, the spatial autocorrelation (Global Moran's I) and high-low clustering (Getis–Ord General G) methods were applied with statistical significance  $p \leq 0.05$ .

## 3. Results

Soil radon concentrations were studied at two Case and Control 1 territories. In the first area, soil VAR varied from 2898.2 to 7137.3 Bq/m<sup>3</sup> (Table 1). The mean value was  $6835.3 \pm 878.3$  Bq/m<sup>3</sup>, with a median value of 5996.4 Bq/m<sup>3</sup>. These data are normally distributed.

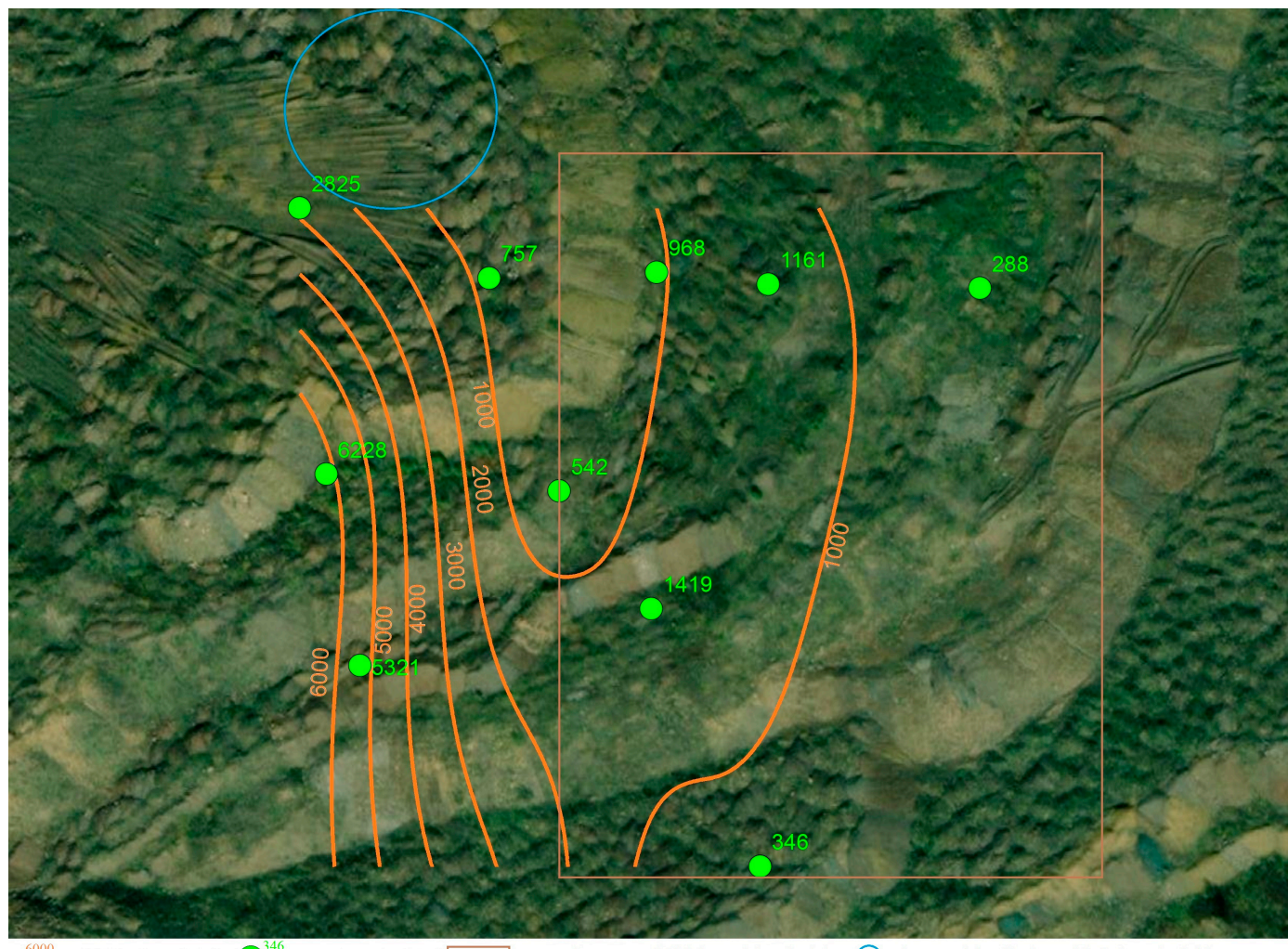
For the Case territory, the soil air VAR varied from 288 to 6228.4 Bq/m<sup>3</sup>, with an average value of 1985.4 Bq/m<sup>3</sup>. These measurements have a non-normal distribution.

In comparison to the Control 1 territory, the radon content in the soil was significantly lower in the Case territory ( $p \leq 0.01$ , M-U test). Some observation points were similar between the two surveyed regions.

Within the Case territory, the radon content in soil air was not homogeneous, and the maximum values were concentrated in the western part of the study area (Figure 4).

**Table 1.** Descriptive analysis of soil air VAR.

No.	Control 1 Territory		Case Territory	
	Soil Radon VAR, Bq/m <sup>3</sup>	SE, Bq/m <sup>3</sup>	Soil Radon VAR, Bq/m <sup>3</sup>	SE, Bq/m <sup>3</sup>
1	5928.4	1777.7	288.0	86.4
2	7934.4	2379.6	1161.0	348.0
3	2898.1	869.4	968.0	290.3
4	4341.4	1301.8	757.0	227.0
5	5996.4	1798.1	542.0	162.5
6	9691.8	2907.1	1419.0	425.0
7	10,035.5	3010.0	346.0	103.8
8	9812.0	2942.9	2825.0	847.2
9	4879.7	1463.3	6228.4	1867.9
10	-	-	5321.0	1595.8



— VAR isolines, Bq/m<sup>3</sup> — research points, Bq/m<sup>3</sup> — approximate area of thick layer of deposited clays — the area of visually observable faults and subsidences

**Figure 4.** Soil air VAR distribution within the Case territory (scale 1:2700).

The meridional elongated shape of anomalies was also observed, corresponding to the shape of anomalies in the soil's radon content.

### 3.1. RFD

Table 2 displays RFD measurements within the three overburden rock massifs.

**Table 2.** Descriptive analysis of RFD.

Research Area	Radon Statistics, $\text{mBq}\cdot\text{m}^{-2}\cdot\text{s}^{-1}$					
	RFD	SE	Mediana	Max	Min	Interval
Control 1	58.97	2.33	57	160	12	148
Control 2	18.36	2.56	12	77	2	75
Case	21	1.93	18.5	53	3	50
All	42.78	1.98	38	160	2	158

A total of 230 sites within three overburden rock massifs were examined. The average RFD for all cases was  $42.78 \pm 1.98 \text{ mBq}\cdot\text{m}^{-2}\cdot\text{s}^{-1}$ , with a range of 2 to  $160 \text{ mBq}\cdot\text{m}^{-2}\cdot\text{s}^{-1}$ . The measurements of RFD do not exhibit a normal distribution.

Differences in RFD in the Case territory from the values in the Control 1 territory were determined by the Mann–Whitney U-test at the significance level below  $p \leq 0.01$ . However, no significant differences were found in the RFD between the Case and Control 2 territories, with a significance level of  $p \geq 0.05$ .

Within the Control 1 territory, there was a rather high level of RFD with an average value of  $58.97 \pm 2.33 \text{ mBq}\cdot\text{m}^{-2}\cdot\text{s}^{-1}$ . At the same time, there were no distinctive tendencies of decrease or increase of radon emanations in the whole territory. The data distribution is non-normal.

RFD for Control 2 territory ranged from 2 to  $77 \text{ mBq}\cdot\text{m}^{-2}\cdot\text{s}^{-1}$ , with an average of  $18.36 \pm 2.56 \text{ mBq}\cdot\text{m}^{-2}\cdot\text{s}^{-1}$ . Low and high RFD regions were observed. The data distribution is non-normal.

RFD at the Case territory averaged  $21 \pm 1.93 \text{ mBq}\cdot\text{m}^{-2}\cdot\text{s}^{-1}$ . The median was  $18.5 \text{ mBq}\cdot\text{m}^{-2}\cdot\text{s}^{-1}$ , with a range of 3 to  $50 \text{ mBq}\cdot\text{m}^{-2}\cdot\text{s}^{-1}$ . The distribution of the data is non-normal. High-value data are clustered around a western part of the studied area (Figure 5) at smaller scales; RFD anomalies exhibit a spotty pattern.

According to the spatial analysis, we obtained clustered data that formed clusters of high values ( $p \leq 0.05$ ). Table 3 presents the results of the study of spatial autocorrelation and high/low radon flux density clusters.

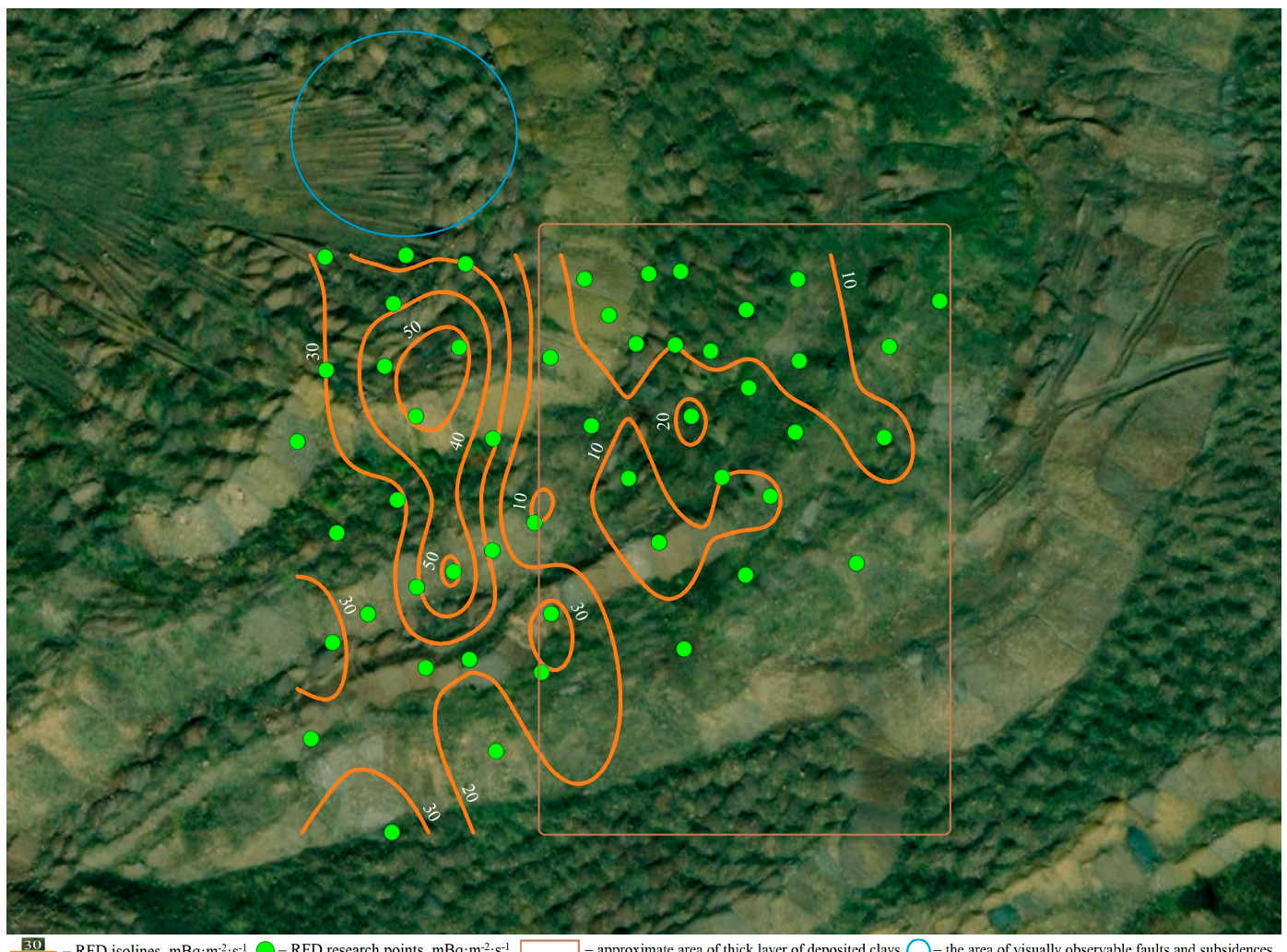


**Figure 5.** RFD distribution within the Case territory (scale 1:2100).

**Table 3.** Descriptive analysis of Global Moran's I and Getis-Ord General G.

	Global Moran's I	Getis-Ord General G
Observed	0.738386	0.005647
Expected	-0.020408	0.004653
Standard Deviation	0.006057	0.000000
z-score	9.750153	2.338623
p-value	0.000000	0.019355

### 3.2. Visual Inspection of the Study Area for the Presence of Fractures

Visual inspection of the study area revealed fractures (presumably detachment fractures) in the body of the massif, which may be permeable zones for gases from the interior of the massif (Figures 6 and 7).

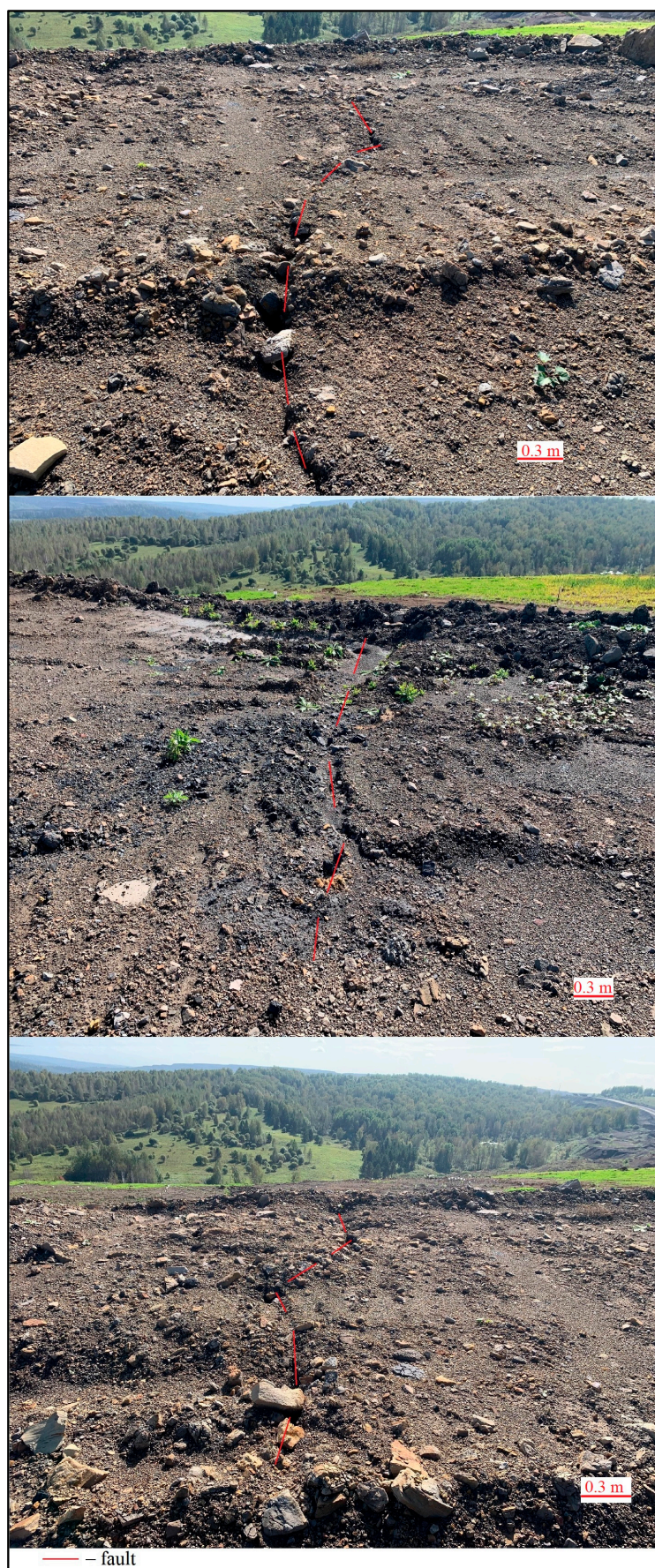


**Figure 6.** Faults on the overburden massif surface.



**Figure 7.** Faults on the overburden massif side. On the left without water outlet; on the right with groundwater outlet.

These fractures were not observed in the part of the massif where a dense clay layer was deposited (Figures 4 and 5). The fractures in the body of the massif mostly extended from north to south throughout the studied massif. There were also areas of subsidence, which were most likely also related to dynamic processes of compaction of the massif body, accompanied by the formation of a new network of fractures (Figure 8). Visually detected faults and subsidence were concentrated in some parts of the study area (Figures 4 and 5).



**Figure 8.** Areas of subsidence.

#### 4. Discussion

The Case territory is characterized by low concentrations of soil radon in comparison with the Control 1 territory. At the same time, the values at some points are comparable with the values of the Control 1 territory. The existence of the obtained spatial heterogeneity of soil radon cannot be explained by differences in the content of  $^{226}\text{Ra}$  in the soil horizon since no significant differences in this parameter were previously found within the study area, as indicated by the data presented in Section 2.

The most probable reason for the observed trends is the better permeability of the western part of the dump massif for gases. This was confirmed by radon flux density data, which also showed higher values in the western part of the investigated area. In this part, there were most likely faults, which appeared in the process of natural movement of the massif after its placement.

At a constant density of gas flow, suitable and produced in the body of the massif, which is in a stressed state, from the bowels of the earth, directly in the body of the massif, the gas will be redistributed along the tension zones, maximum, and through compression zones, minimum. The sedimentary section of the massif is generally under high tension due to the pores closing or being occupied by adsorbed or film water. As is known from previous studies, degassing of the massif occurs through weakened zones or fractures that are formed during the movement of the massif. This assumption is also supported by the presence of north–south elongated isolines reflecting methane leakage in the massif body, as shown in Figure 3. This shape most likely reflects the presence of multiple degassing systems in the massif along these meridionally oriented fractures. Stretch or fault zones have a subvertical position. Previous studies on the migration of gases from the geological environment have given a special role to methane and other gases of the lithosphere in the transport of radon gas to the surface [27,28,45]. This also confirms our conclusion regarding the coincidence of the forms of radon and methane anomalies.

On the surface of the massif and its walls, we found zones of faults (Figures 6 and 7), most likely due to detachment and small surface subsidence that occurred after the formation of the dump. These processes are natural for most overburden rock massifs, and their development ceases when the movement of the massif ceases [46,47]. Multiple freeze–thaw cycles can prolong this process [48]. Formed systems of detachment fractures and more localized structures near small areas of surface subsidence can form surface gas anomalies of linear shape in the first case and ring shape in the second. The direction of extension of these fractures coincides with the direction of pulling anomalies, i.e., coincides with the meridional direction. These violations of massif continuity act as channels of massif degassing. At present, there is no movement of the massif, but for the prediction of catastrophic processes, monitoring is necessary, which is possible using gas dynamic data, similar to previous studies on natural and anthropogenic landslides [49]. The overlying layer of dense clay affected the results of the radon and soil radon flux density measurements because it formed a sufficiently dense screen for gases from the landfill atmosphere. Weakened fault zones within the massif may no longer develop as fault zones, but they can still enhance water erosion, leading to the creation of deep ravines [50]. We did not observe any visual faults in this layer, indicating the stability of the dump massif after the application of this clay layer.

It is well known that coal mine overburden rock massifs are prone to spontaneous combustion [51]. This leads to an increase in the emission of gases to the surface and changes in the temperature of the massif body. Moreover, the long burning process interferes with the process of biological reclamation of the overburden rock massifs, which requires the obligatory elimination of fire centers in the body of the massif. In our case, these processes are not observed, as can be seen in Figure 2, and this process could not stimulate the release of radon to the surface. However, spontaneous combustion can start later, and the beginning of its process can be determined by monitoring the gas emission to the surface. The change in gas concentration in the body of the massif can indicate dynamic processes in its internal parts. In this case, the temperature of the body of the overburden rock massifs

changes a little later. The mobility of the massif and its spontaneous combustion may be determined by its location in a tectonic fault zone [52].

Low values of RFD indicate the presence of a shield for radon from deeper horizons, so the radon level is determined by its diffusion from the applied clays, namely radium content, porosity, and moisture. Close values of radon flux density between Control 2 territory and Case territory indicate the similar composition of the studied massifs and the presence of a dense clay layer for the studied area. The overburden rock massifs in Control 1 territory are characterized by the technology of stockpiling and the absence of an anthropogenic clay horizon between the dumped rocks and the rocks on which the dump was placed. This situation also affected the radon content of the soil in the upper horizon of the overburden rock massifs in the Control 1 territory.

Studying the release of gases from dump areas will make it possible to predict negative processes for plant communities formed independently or in the process of reclamation [37,53,54]. As is known from previous studies, vegetation cover has a significant connection with the areas of degassing of the massif, as well as with its temperature characteristics, which can change sharply during the process of spontaneous combustion of the dump mass [38–40]. Thus, monitoring the gas atmosphere of the dump area is necessary.

In conclusion, we recommend continued visual observations on the massif body after spring flooding, electrical surveys to identify possible water-bearing areas and potential slip mirrors, and radon monitoring with more soil radon observations to elucidate gas dynamics in the massif body.

## 5. Conclusions

A heterogeneous radon field was observed within the investigated overburden rock massif. Maximum VAR and RFD were detected alongside visually observed zones of faults and subsidence. These zones are permeable zones for gases of the overburden rock massif. The forms of gas emission anomalies (methane, radon) within the massif coincide with the extension of the fault zones. This fracturing was not observed on the formed layer of dense clays, which may indicate that the movement of the massif has stopped. As a recommendation, we would suggest determining the electrical resistivity of the rocks of the massif body using the electrical tomography method in order to identify the watered zones of the massif body and the wetting conditions of potential displacement lines. With regard to radon monitoring, a system of stations should be installed to record the concentration of radon in soil air constantly in order to clarify the spatial characteristics of gas emission from the body of the massif. A dense clay layer is a potentially suitable way to isolate the body of a massif from the external atmosphere.

In the process of our work, we came to the conclusion that, to reduce the impact of emitted gases and the possibility of burning the massif, it is necessary to tightly isolate the inner part of the massif from atmospheric gases. Long-term monitoring of radon allows us to determine the dynamics of the overburden rock massif, including combustion processes. Radon as an indicator gas of fires, the presence of permeable zones, and dynamic processes in the body of the overburden rock massif confirmed its usefulness in this study.

**Author Contributions:** Conceptualization, T.L.; Formal analysis, A.L., E.N., P.K. and K.L.; Funding acquisition, P.K.; Investigation, T.L. and K.L.; Methodology, T.L.; Project administration, P.K.; Supervision, A.L. and E.N.; Validation, E.N. and K.L.; Visualization, T.L.; Writing—original draft, T.L. and A.L.; Writing—review and editing, T.L. All authors have read and agreed to the published version of the manuscript.

**Funding:** The research was conducted as part of the comprehensive scientific and technical program of a complete innovative cycle “Development and implementation of a complex of technologies in the fields of exploration and extraction of minerals, ensuring of industrial safety, bioremediation, creation of new products of deep processing of coal raw materials with consecutive amelioration of ecological impact on the environment and risks to human life”, approved by the Decree of the Government of the Russian Federation from 11.05.2022 No. 1144-r. Agreement No. 075-15-2022-1200 dated 28 September 2022.

**Data Availability Statement:** The data presented in this study are available in article.

**Conflicts of Interest:** The authors declare no conflicts of interest.

## References

- Bazaluk, O.; Anisimov, O.; Saik, P.; Lozynskyi, V.; Akimov, O.; Hrytsenko, L. Determining the Safe Distance for Mining Equipment Operation When Forming an Internal Dump in a Deep Open Pit. *Sustainability* **2023**, *15*, 5912. [[CrossRef](#)]
- Prokopenko, S.A.; Ludzish, V.S.; Lesin, Y.V.; Tyulenev, M.A.; Sushko, A.V. Structural Peculiarities of Coal Mine Waste Piles in Kuzbass. *J. Min. Sci.* **2017**, *53*, 92–98. [[CrossRef](#)]
- Makridin, E.V.; Tyulenev, M.A.; Markov, S.O.; Lesin, Y.V.; Murko, E.V. Overburden management towards higher safety in coal mining regions. *Min. Informational Anal. Bull.* **2020**, *12*, 89–102. [[CrossRef](#)]
- Cheskivov, V.I.; Bobylsky, A.S. Technology and Ecology of Dumping at Open Pit Mines in Kuzbass. *J. Min. Sci.* **2017**, *53*, 882–889. [[CrossRef](#)]
- Makridin, E.V.; Tyulenev, M.A.; Markov, S.O. Experimental study of the quarry wastewater filtering in coarse-grained massifs of rock debris at kamyshansky open pit mine. *Teh. Tehnol. Gorn. Dela* **2020**, *2*, 4–25. [[CrossRef](#)]
- Tyulenev, M.A.; Markov, S.O.; Gasanov, M.A.; Zhironkin, S.A. Numerical Modeling in the Structural Study of Technogenic Rock Array. *Geotech. Geol. Eng.* **2018**, *36*, 2789–2797. [[CrossRef](#)]
- Ivanova, S.; Vesnina, A.; Fotina, N.; Prosekov, A. An Overview of Carbon Footprint of Coal Mining to Curtail Greenhouse Gas Emissions. *Sustainability* **2022**, *14*, 15135. [[CrossRef](#)]
- Amrani, M.; Taha, Y.; El Haloui, Y.; Benzaazoua, M.; Hakkou, R. Sustainable Reuse of Coal Mine Waste: Experimental and Economic Assessments for Embankments and Pavement Layer Applications in Morocco. *Minerals* **2020**, *10*, 851. [[CrossRef](#)]
- Amrani, M.; Taha, Y.; Kchikach, A.; Benzaazoua, M.; Hakkou, R. Field and Economic Studies on Mine Waste: Sustainable Reuse as Aggregates for Low Traffic Pavement Structure. *Sustainability* **2022**, *14*, 12540. [[CrossRef](#)]
- do Amaral Filho, J.R.; Gcayiya, M.; Kotsopoulos, A.; Broadhurst, J.L.; Power, D.; Harrison, S.T.L. Valorization of South African Coal Wastes through Dense Medium Separation. *Minerals* **2022**, *12*, 1519. [[CrossRef](#)]
- Khalil, A.; Taha, Y.; Benzaazoua, M.; Hakkou, R. Applied Methodological Approach for the Assessment of Soil Contamination by Trace Elements around Abandoned Coal Mines—A Case Study of the Jerada Coal Mine, Morocco. *Minerals* **2023**, *13*, 181. [[CrossRef](#)]
- Mishra, A.; Das, S.K.; Reddy, K.R. Processing Coalmine Overburden Waste Rock as Replacement to Natural Sand: Environmental Sustainability Assessment. *Sustainability* **2022**, *14*, 14853. [[CrossRef](#)]
- Luo, H.; Zhou, W.; Jiskani, I.M.; Wang, Z. Analyzing Characteristics of Particulate Matter Pollution in Open-Pit Coal Mines: Implications for Green Mining. *Energies* **2021**, *14*, 2680. [[CrossRef](#)]
- Wang, Z.; Zhou, W.; Jiskani, I.M.; Luo, H.; Ao, Z.; Mvula, E.M. Annual Dust Pollution Characteristics and Its Prevention and Control for Environmental Protection in Surface Mines. *Sci. Total Environ.* **2022**, *825*, 153949. [[CrossRef](#)]
- Leshukov, T.; Legoshchin, K.; Yakovenko, O.; Bach, S.; Russakov, D.; Dimakova, D.; Vdovina, E.; Baranova, E.; Avdeev, K.; Kolpina, E.; et al. Fractional Composition and Toxicity Coal-Rock of PM10-PM0.1 Dust near an Opencast Coal Mining Area and Coal-Fired Power Station. *Sustainability* **2022**, *14*, 16594. [[CrossRef](#)]
- Park, I.; Tabelin, C.B.; Jeon, S.; Li, X.; Seno, K.; Ito, M.; Hiro Yoshi, N. A Review of Recent Strategies for Acid Mine Drainage Prevention and Mine Tailings Recycling. *Chemosphere* **2019**, *219*, 588–606. [[CrossRef](#)]
- Marove, C.A.; Sotozono, R.; Tangviroon, P.; Tabelin, C.B.; Igarashi, T. Assessment of Soil, Sediment and Water Contaminations around Open-Pit Coal Mines in Moatize, Tete Province, Mozambique. *Environ. Adv.* **2022**, *8*, 100215. [[CrossRef](#)]
- Pondja, E.A.; Persson, K.M.; Matsinhe, N.P. Assessment of Coal Mine Water in Moatize by Static and Leaching Tests. *Sustain. Water Resour. Manag.* **2017**, *3*, 403–412. [[CrossRef](#)]
- Marove, C.A.; Tangviroon, P.; Tabelin, C.B.; Igarashi, T. Leaching of Hazardous Elements from Mozambican Coal and Coal Ash. *J. Afr. Earth Sci.* **2020**, *168*, 103861. [[CrossRef](#)]
- Silva, N.C.; Chagas, E.G.L.; Abreu, C.B.; Dias, D.C.S.; Lopez, D.; Guerreiro, E.T.Z.; Alberti, H.L.C.; Braz, M.L.; Branco, O.; Fleming, P. Radon as a Natural Tracer for Gas Transport within Uranium Waste Rock Piles. *Radiat. Prot. Dosim.* **2014**, *160*, 74–77. [[CrossRef](#)]
- Fabiańska, M.J.; Ciesielczuk, J.; Kruszewski, Ł.; Misz-Kennan, M.; Blake, D.R.; Stracher, G.; Moszumańska, I. Gaseous Compounds and Efflorescences Generated in Self-Heating Coal-Waste Dumps—A Case Study from the Upper and Lower Silesian Coal Basins (Poland). *Int. J. Coal Geol.* **2013**, *116–117*, 247–261. [[CrossRef](#)]
- Hu, X.; Sun, Q.; Shi, Q.; Wang, N.; Geng, J.; Xue, S. Radon Exhalation Characteristics after Pyrolysis of Long Flame Coal. *Sci. Total Environ.* **2023**, *904*, 167228. [[CrossRef](#)]
- Ribeiro, J.; Suárez-Ruiz, I.; Flores, D. Coal Related Fires in Portugal: New Occurrences and New Insights on the Characterization of Thermally Affected and Non-Affected Coal Waste Piles. *Int. J. Coal Geol.* **2022**, *252*, 103941. [[CrossRef](#)]
- Carras, J.N.; Day, S.J.; Saghafi, A.; Williams, D.J. Greenhouse Gas Emissions from Low-Temperature Oxidation and Spontaneous Combustion at Open-Cut Coal Mines in Australia. *Int. J. Coal Geol.* **2009**, *78*, 161–168. [[CrossRef](#)]
- Nádudvari, Á.; Cabała, J.; Marynowski, L.; Jabłońska, M.; Dziurowicz, M.; Malczewski, D.; Koziełska, B.; Siupka, P.; Piotrowska-Seget, Z.; Simoneit, B.R.T.; et al. High Concentrations of HgS, MeHg and Toxic Gas Emissions in Thermally Affected Waste Dumps from Hard Coal Mining in Poland. *J. Hazard. Mater.* **2022**, *431*, 128542. [[CrossRef](#)]

26. Liang, Y.; Liang, H.; Zhu, S. Mercury Emission from Spontaneously Ignited Coal Gangue Hill in Wuda Coalfield, Inner Mongolia, China. *Fuel* **2016**, *182*, 525–530. [[CrossRef](#)]
27. Etiope, G.; Lombardi, S. Evidence for Radon Transport by Carrier Gas through Faulted Clays in Italy. *J. Radioanal. Nucl. Chem. Artic.* **1995**, *193*, 291–300. [[CrossRef](#)]
28. Cvetković, M.; Kapuralić, J.; Pejić, M.; Kolenković Močilac, I.; Rukavina, D.; Smirčić, D.; Kamenski, A.; Matoš, B.; Špelić, M. Soil Gas Measurements of Radon, CO<sub>2</sub> and Hydrocarbon Concentrations as Indicators of Subsurface Hydrocarbon Accumulation and Hydrocarbon Seepage. *Sustainability* **2021**, *13*, 3840. [[CrossRef](#)]
29. Dyck, W.; Jonasson, I.R. Chapter 11 Radon. In *Handbook of Exploration Geochemistry*; Hale, M., Ed.; Geochemical Remote Sensing of the Sub-Surface; Elsevier Science B.V.: Amsterdam, The Netherlands, 2000; Volume 7, pp. 353–394.
30. Wang, S.; Luo, K.; Wang, X.; Sun, Y. Estimate of Sulfur, Arsenic, Mercury, Fluorine Emissions Due to Spontaneous Combustion of Coal Gangue: An Important Part of Chinese Emission Inventories. *Environ. Pollut.* **2016**, *209*, 107–113. [[CrossRef](#)]
31. Tan, B.; Zhang, F.; Zhang, Q.; Wei, H.; Shao, Z. Firefighting of Subsurface Coal Fires with Comprehensive Techniques for Detection and Control: A Case Study of the Fukang Coal Fire in the Xinjiang Region of China. *Environ. Sci. Pollut. Res.* **2019**, *26*, 29570–29584. [[CrossRef](#)]
32. Liu, Y.G.; Yu, L.N.; Wang, H.C. Study on Countermeasures of Coal Gangue Pollution Prevention and Regional Sustainable Development in China. *Appl. Mech. Mater.* **2013**, *307*, 510–513. [[CrossRef](#)]
33. Shao, Z.; Wang, D.; Cao, K.; Si, W.; Li, Y.; Liu, J. Treatment of Smouldering Coal Refuse Piles: An Application in China. *Environ. Technol.* **2020**, *41*, 3105–3118. [[CrossRef](#)]
34. Zhao, P.; Zhuo, R.; Li, S.; Lin, H.; Shu, C.-M.; Shuang, H.; Wei, Z. Greenhouse Gas Protection and Control Based upon the Evolution of Overburden Fractures under Coal Mining: A Review of Methods, Influencing Factors, and Techniques. *Energy* **2023**, *284*, 129158. [[CrossRef](#)]
35. World Health Organization. *WHO Handbook on Indoor Radon: A Public Health Perspective*; World Health Organization: Geneva, Switzerland, 2009; ISBN 978-92-4-154767-3.
36. Hong, Y.; Du, H.; Chen, M. Bearing Capacity Analysis of the Weak Basement, Progressive Destruction Analysis, and Evaluation of the Dump on an Inclined Strip Section Using the Upper-Limit Method: A Case Study in an Anonymous Open-Cast Coal Mine. *Sustainability* **2023**, *15*, 10240. [[CrossRef](#)]
37. Ren, H.; Zhao, Y.; Xiao, W.; Yang, X.; Ding, B.; Chen, C. Monitoring Potential Spontaneous Combustion in a Coal Waste Dump after Reclamation through Unmanned Aerial Vehicle RGB Imagery Based on Alfalfa Aboveground Biomass. *Land Degrad. Dev.* **2022**, *33*, 2728–2742. [[CrossRef](#)]
38. Ren, H.; Xiao, W.; Zhao, Y. Examining the Effect of Spontaneous Combustion on Vegetation Restoration at Coal Waste Dumps after Reclamation: Taking *Medicago sativa* L. (Alfalfa) as an Indicator. *Sci. Total Environ.* **2023**, *901*, 165668. [[CrossRef](#)]
39. Abramowicz, A.; Rahmonov, O.; Chybiorz, R.; Ciesielczuk, J. Vegetation as an Indicator of Underground Smouldering Fire on Coal-Waste Dumps. *Fire Saf. J.* **2021**, *121*, 103287. [[CrossRef](#)]
40. Ren, H.; Zhao, Y.; Xiao, W.; Zhang, J.; Chen, C.; Ding, B.; Yang, X. Vegetation Growth Status as an Early Warning Indicator for the Spontaneous Combustion Disaster of Coal Waste Dump after Reclamation: An Unmanned Aerial Vehicle Remote Sensing Approach. *J. Environ. Manag.* **2022**, *317*, 115502. [[CrossRef](#)]
41. Osintseva, M. Assessment of Soil Properties in Technogenically Disturbed Lands of Kemerovo Oblast—Kuzbass. *Qubahan Acad. J.* **2023**, *3*, 77–92. [[CrossRef](#)]
42. Podurets, O.I. Spatial variability of the content of heavy metals in the soil cover under the influence of a coal mining enterprise. *Ugol'* **2023**, *10*, 51–58. [[CrossRef](#)]
43. Shao, Z.; Deng, R.; Zhang, G.; Li, Y.; Tang, X.; Zhang, W. 3D Thermal Mapping of Smouldering Coal Gangue Pile Fires Using Airborne Thermal Infrared Data. *Case Stud. Therm. Eng.* **2023**, *48*, 103146. [[CrossRef](#)]
44. Zubíček, V.; Hudeček, V.; Orlíková, L.; Dandoš, R.; Jadvíščok, P.; Adjiski, V.; Dlouhá, D. Thermal Signatures of Relict Coal Spoil, Waste and Tailing Dumps. *Int. J. Min. Reclam. Environ.* **2023**, *1*–13. [[CrossRef](#)]
45. Portola, V.A.; Tailakov, O.V.; Lee, H.U.; Sobolev, V.V.; Bobrovnikova, A.A. Detection, location and assessment of underground fires using radon anomalies on the day surface. *Ugol'* **2021**, *47*–52. [[CrossRef](#)]
46. Tovele, G.S.V.; Han, L.; Shu, J.S. Variation of Open-Pit Waste Dump Specimens Under Effective Pressure Influence. *Front. Earth Sci.* **2021**, *8*, 582918. [[CrossRef](#)]
47. Upadhyay, O.P.; Sharma, D.K.; Singh, D.P. Factors Affecting Stability of Waste Dumps in Mines. *Int. J. Surf. Min. Reclam. Environ.* **1990**, *4*, 95–99. [[CrossRef](#)]
48. Deng, H.; Zhao, B.; Xiao, Y.; Tian, G. Experimental Study on Macroscopic Mechanical Characteristics and Microscopic Pore Structure Evolution of Soil–Rock Mixture under Repeated Freeze–Thaw Cycles. *Appl. Sci.* **2023**, *13*, 11504. [[CrossRef](#)]
49. Zaalistvili, V.; Melkov, D.; Revazov, M. Relationship of radon emanation with the level of external impact according to large landslides monitoring in mountain areas. *Sustain. Dev. Mt. Territ.* **2021**, *13*, 564–575. [[CrossRef](#)]
50. Li, Y.; Lv, G.; Wang, D.; Su, W.; Wei, Z. Erosion Failure of Slope in a Dump with Ground Fissure under Heavy Rain. *Water* **2022**, *14*, 3425. [[CrossRef](#)]
51. Misz-Kennan, M.; Tabor, A. Chapter 15—The Thermal History of Select Coal-Waste Dumps in the Upper Silesian Coal Basin, Poland. In *Coal and Peat Fires: A Global Perspective*; Stracher, G.B., Prakash, A., Sokol, E.V., Eds.; Elsevier: Boston, MA, USA, 2015; pp. 431–462. ISBN 978-0-444-59509-6.

52. Musina, V.R.; Golovko, I.V.; Shermatova, S. Type of Crossing of Coal Waste Dumps by Geodynamical Dangerous Zones. *MIAB. Min. Inf. Anal. Bull.* **2020**, 233–241. [[CrossRef](#)]
53. Kumar, A.; Das, S.K.; Nainegali, L.; Reddy, K.R. Phytostabilization of Coalmine Overburden Waste Rock Dump Slopes: Current Status, Challenges, and Perspectives. *Bull. Eng. Geol. Environ.* **2023**, 82, 130. [[CrossRef](#)]
54. Radosz, Ł.; Chmura, D.; Prostański, D.; Woźniak, G. The Soil Respiration of Coal Mine Heaps’ Novel Ecosystems in Relation to Biomass and Biotic Parameters. *Energies* **2023**, 16, 7083. [[CrossRef](#)]

**Disclaimer/Publisher’s Note:** The statements, opinions and data contained in all publications are solely those of the individual author(s) and contributor(s) and not of MDPI and/or the editor(s). MDPI and/or the editor(s) disclaim responsibility for any injury to people or property resulting from any ideas, methods, instructions or products referred to in the content.